PARAMETRIC REDUCED ORDER MODEL FOR RAPID PREDICTION OF DYNAMIC LOADS AND AEROELASTIC RESPONSE WITH STRUCTURAL NONLINEARITIES

Michele Castellani[1,2], Yves Lemmens[1], Jonathan E. Cooper[2]

[1] Aerospace Centre of Competence
Siemens PLM Software Belgium
Interleuvenlaan 68, 3001 Leuven, Belgium
michele.castellani@siemens.com

[2] Department of Aerospace Engineering
University of Bristol
Queen's Building, University Walk, BS8 1TR Bristol, UK
j.e.cooper@bristol.ac.uk

Keywords: aircraft loads, flexible aircraft, Parametric ROM, nonlinear aeroelasticity, load alleviation

Abstract: This paper presents a procedure based on Parametric Model Order Reduction of a state-space aeroservoelastic system aimed at reducing the computational time associated to perform flight loads calculation across the flight envelope. It is shown that the method determines accurate predictions of both peak and correlated loads with a significant saving in computational time. The procedure is extended to simulate aeroelastic systems with concentrated structural nonlinearities and applied to the multi-objective optimisation of a wing tip device for load alleviation featuring a nonlinear stiffness element.

1 INTRODUCTION

Loads calculations play an important part across much of the design and development of an aircraft, and have an impact upon structural design, aerodynamic characteristics, weight, flight control system design and performance. The certification of large commercial aircraft is covered by the EASA CS-25 [1]. Loads requirements are defined in the context of the flight envelope. The regulations require that enough points within the flight envelope are investigated to ensure that the critical loads for each part of the aircraft are identified. The flight conditions which provide the largest aircraft loads are not known a-priori. Therefore the aerodynamic and inertial forces have to be calculated at a large number of conditions to give an estimate of the maximum loads, and hence stresses, that the aircraft will experience in service. It is of great interest for aircraft design to identify which are the critical loading events and at what design configuration and flight conditions they occur. A typical aircraft loads design process involves monitoring many of so-called Interesting Quantities (IQs) (e.g. bending moments, torques, accelerations etc.) for a wide range of different load cases that the aircraft is likely to experience in-flight and on the ground. Each "loads loop" simulates the response of a numerical aeroelastic aircraft model to these loads and determine the critical cases, and these results are fed into the structural design. Such a process is extremely time consuming and furthermore, has to be repeated every time that there is an update in the aircraft structure.

It is usual to determine the extreme loads cases for 1D (single IQs) and 2D (correlated IQs) events. In the latter case, pairs of IQ response time histories are plotted against each other for a range of different load cases. The extreme vertices of the envelope encompassing these plots determine the critical load cases that are then used to perform stress calculations. Previous work in the FFAST EU FP7 project [2] investigated the use of several surrogate models and optimisation methods for fast and efficient prediction of the worst case gust loads for each IQ of a large transport aircraft model. It was shown that considerable savings in computational time can be made without sacrificing accuracy; however, the IQs were dealt with independently. Recent work [5] has investigated an approach to determine surrogate models of correlated loads based upon the use of the Singular Value Decomposition. A great deal of work has been presented in the past investigating the effect of nonlinearities such as freeplay on the aeroelastic stability of control surfaces [6] whereas little effort has been devoted to the effect of nonlinearities on loads.

In this paper, an approach for rapid loads estimation based on Parametric Model Order Reduction (PMOR) will be described. It produces a Reduced Order Model (ROM) able to predict IQs time histories for different flight conditions retaining a good accuracy with a significant reduction in computational time. The effectiveness of the developed method is demonstrated by considering loads due to gusts and pitching manoeuvres for an aeroservoelastic model of a generic transport aircraft. The PMOR approach is then extended to simulate the gust response of an aeroelastic system with concentrated structural nonlinearities. A passive wing tip device for load alleviation connected to the wing via a nonlinear flexible element is studied and a multi-objective optimisation performed applying the PMOR procedure proposed, which proves to be effective and computationally efficient.

2 AEROSERVOELASTIC MODEL

The method described in this paper has been applied to the discrete gust response and pitching manoeuvre simulation of a generic transport aircraft, representative of a modern airliner, whose main features are summarized in Table 1.

Property	**Value**
Wingspan	65*m*
MTOW	268*tons*
Max operating altitude	43000*ft*
V_A-M_A	142*m/s*-0.82
V_C-M_C	172*m/s*-0.89
V_D-M_D	188*m/s*-0.95
$n_{z,max}$	2.5*g*
$n_{z,min}$	-1*g*

Table 1: Main features of the aircraft model

The aircraft model was developed as part of the FFAST FP7 project and is shown in Figure 1. The structural model is a FE stick model where the fuselage, wing, tailplanes and engine pylons are represented by beam elements in the FE solver Nastran. The model includes both distributed and lumped masses for the systems, furniture, payload, fuel and engines. The

aerodynamic model is a Doublet Lattice Method (DLM) [7] mesh where each lifting surface is modelled as a flat plate. The control surfaces are modelled only in the aerodynamic mesh as if being controlled through servo-hydraulic actuators, whose transfer functions are known following a linearization of the originally nonlinear equations about the neutral operating point.

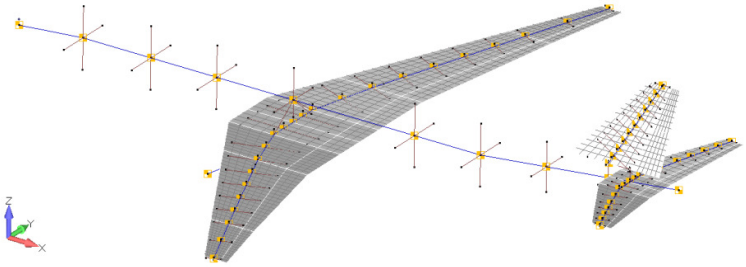

Figure 1: Structural and aerodynamic model of the generic transport aircraft

3 AEROSERVOELASTIC EQUATIONS OF MOTION

The linear aeroelastic equations of motion in generalized coordinates, excited by atmospheric gust and control surfaces, are formulated in the Laplace domain as

$$\left(s^2\boldsymbol{M_{hh}} + s\boldsymbol{C_{hh}} + \boldsymbol{K_{hh}} - q_\infty \boldsymbol{Q_{hh}}(p,M)\right)\boldsymbol{q_h}(s) = q_\infty \boldsymbol{Q_{hg}}(p,M)w_g(s)/V + q_\infty \boldsymbol{Q_{hc}}(p,M)\boldsymbol{\delta}(s) \qquad (1)$$

where the generalized coordinates $\boldsymbol{q_h}$ could be either a low-frequency subset of the normal modes of the structure or a finite number of assumed deformation shapes. The Generalized Aerodynamics Forces (GAF) matrices $\boldsymbol{Q_{hh}}$, $\boldsymbol{Q_{hg}}$ and $\boldsymbol{Q_{hc}}$ related respectively to structural motion, gust and control surfaces deflection, are obtained by DLM and are tabulated at specific Mach numbers and reduced frequencies k. The gust velocity profile w_g represents the external excitation. The effects of the servo-hydraulic actuators driving the control surfaces are included assuming a 3rd order transfer function between the commanded input of the pilot u_c and the actual control surface deflection δ [8].

The aeroelastic equations of motion can be directly solved in the frequency-domain and the time histories of the IQs obtained through application of the Inverse Fourier Transform. To apply the Parametric Model Order Reduction method presented in this paper; however, Eq. (1) must be translated into the time-domain and cast in state-space form, leading to a Linear Time Invariant (LTI) system

$$\begin{aligned} \dot{\boldsymbol{x}}_{\boldsymbol{ae}} &= \boldsymbol{A_{ae}}\boldsymbol{x_{ae}} + \boldsymbol{B_{ae}}\boldsymbol{u} \\ \boldsymbol{y} &= \boldsymbol{C_{ae}}\boldsymbol{x_{ae}} + \boldsymbol{D_{ae}}\boldsymbol{u} \end{aligned} \qquad (2)$$

Since the GAF matrices are only available at a discrete set of reduced frequencies, in order to obtain a time-domain representation of the aeroelastic system, the tabulated GAF matrices are used to compute a Rational Function Approximation (RFA) of the aerodynamics in the entire Laplace domain, which is given by

$$\begin{aligned} \widetilde{\boldsymbol{Q_{hh}}}(s,M) &= \boldsymbol{D_0} + \tfrac{l_a}{V}\boldsymbol{D_1}s + \left(\tfrac{l_a}{V}\right)^2 \boldsymbol{D_2}s^2 + \boldsymbol{C_a}\left(s\boldsymbol{I} - \tfrac{V}{l_a}\boldsymbol{A_a}\right)\boldsymbol{B_a}s \\ \widetilde{\boldsymbol{Q_{hg}}}(s,M) &= \boldsymbol{D_{0g}} + \tfrac{l_a}{V}\boldsymbol{D_{1g}}s + \left(\tfrac{l_a}{V}\right)^2 \boldsymbol{D_{2g}}s^2 + \boldsymbol{C_g}\left(s\boldsymbol{I} - \tfrac{V}{l_a}\boldsymbol{A_g}\right)\boldsymbol{B_g}s \end{aligned} \qquad (3)$$

Eq. (3) results in the augmented aerodynamic and gust state vectors $\boldsymbol{x_a}$ and $\boldsymbol{x_g}$ in the state-space system of Eq. (2) (refer to [9] for the assembly of the matrices). The unsteady GAF of the control surfaces are instead cast into the time-domain through a quasi-steady approximation, which reads

$$\widetilde{\boldsymbol{Q_{hc}}}(s,M) = \boldsymbol{D_{0c}} + \frac{l_a}{V}\boldsymbol{D_{1c}}s + \left(\frac{l_a}{V}\right)^2 \boldsymbol{D_{2c}}s^2 = \boldsymbol{Q_{hc}}(0,M) + \frac{l_a}{V}\boldsymbol{Q'_{hc}}(0,M)s + \frac{1}{2}\left(\frac{l_a}{V}\right)^2 \boldsymbol{Q''_{hc}}(0,M)s^2 \quad (4)$$

The control surface deflections are linked to the pilot input command u_c via the actuator transfer function. Expressing the state-space realization of the latter in controllable canonical form adds three states to the aeroelastic system and the input vector $\boldsymbol{u}$ thus contains the gust velocity w_g, its first time derivative $\dot{w}_g$ and the pilot commanded input u_c. The output vector $\boldsymbol{y}$ contains the IQs, which are recovered through the mode displacement method.

3.1 Optimised Least-Squares Rational Function Approximation

Many approaches have been developed to perform the approximation of the tabulated GAF by rational polynomials in the Laplace domain [9]. In this work, Roger's method [10] is used, which assumes the following representation of Eq. (3) as

$$\widetilde{\boldsymbol{Q_{hh}}}(s,M) = \boldsymbol{D_0} + \frac{l_a}{V}\boldsymbol{D_1}s + \left(\frac{l_a}{V}\right)^2 \boldsymbol{D_2}s^2 + \frac{V}{l_a}\sum_{l=1}^{n_a} \frac{s}{s+{}^{V}/_{l_a}\beta_l}\boldsymbol{A_l} \quad (5)$$

In the original formulation the number and values of aerodynamic poles β_l are fixed a-priori by the user in the range of reduced frequencies of interest, imposing that $\beta_l > 0$ to ensure asymptotic stability, and the unknowns are the coefficients of the matrices appearing at the numerator. These are determined by a linear least-square curve fit carried out term-by-term on each coefficient of the tabulated $\boldsymbol{Q_{hh}}$. The GAF of the gust, $\boldsymbol{Q_{hg}}$, is approximated independently with the same expression. This approach allows for a greater flexibility in the selection of the gust aerodynamic poles and increases the fitting accuracy, an important consideration because the gust GAF is known to show a spiral behaviour at high reduced frequencies in the Re-Im plane, difficult to approximate with rational polynomials, due to the penetration term [13]. Although the choice of Roger's RFA and the independent fitting of the gust GAF leads to a state-space model whose size is greater compared to the Minimum-State method by Karpel [9], the model is afterwards reduced to a considerably smaller size through Model Order Reduction. Moreover, Roger's RFA is robust and offers less computational burden than the Minimum-State method [14], even though this cost, if a MOR is not subsequently carried out, is ultimately overcome by a smaller resulting model employed in the simulations.

The original formulation by Roger is extended considering the aerodynamic poles as free design variables of an optimisation process, whose objective function is the minimization of the squared error between the approximated and tabulated GAF. This approach gives an additional degree of freedom in obtaining good curve-fits, particularly for the gust GAF, for a small increase in computational cost. It also allows adapting the RFA to each Mach number of interest, since commonly, in the unoptimised approach, the poles are held arbitrarily constant over a range of Mach numbers, whereas the GAF can change significantly with Mach number. Several studies have been presented on nonlinear optimisation of the aerodynamic poles [14]. In this work, an optimisation is performed to select the poles minimizing the functional

$$\mathcal{F} = \sum_{j=1}^{n_h} \left(\sum_{i=1}^{n_h} \sum_{m=1}^{n_k} w_{ij} \varepsilon_{ijm} \right)^{1/2}$$
$$\varepsilon_{ij} = \frac{|\widetilde{Q_{ij}} - Q_{ij}|^2}{max_m\{1, |Q_{ij}|^2\}} \tag{6}$$

where w_{ij} are weighting factors that can be chosen if some specific elements of the $\boldsymbol{Q_{hh}}$ are deemed more important to approximate accurately. The whole RFA procedure consists therefore of a two-level optimisation: an inner linear least-square curve fitting for the coefficients matrices at the numerator of Eq. (5) and an outer nonlinear optimisation for the aerodynamic poles β_l.

Because the aerodynamic poles appear in the denominator of Eq. (5), when these are chosen as variables in a gradient-based optimisation method, there could be difficulties in computing the gradient and issues with the stability and convergence of the optimiser. For this reason, three non-gradient optimisation algorithms are employed and compared: a Nelder-Mead simplex scheme, a genetic algorithm and simulated annealing. As indicator of the goodness of the fit, the total root mean square error is calculated

$$ERR = \frac{1}{\sqrt{n_k}} \sum_{j=1}^{n_h} \left(\sum_{i=1}^{n_h} \sum_{m=1}^{n_k} w_{ij} \varepsilon_{ijm} \right)^{1/2} \tag{7}$$

The unoptimised and optimised RFAs are performed on the aeroservoelastic model from $\boldsymbol{Q_{hh}}$ and $\boldsymbol{Q_{hg}}$ generated by DLM at a Mach number of 0.60. Table 2 reports the total root mean square error of $\boldsymbol{Q_{hh}}$ and $\boldsymbol{Q_{hg}}$ obtained with the standard (unoptimised) RFA and the RFA with the aforementioned optimisation algorithms assuming 5 and 6 aerodynamic poles respectively. For the same number of aerodynamic states, there is an improvement of the approximation optimising the poles location. Notably, due to the spiral nature of the gust GAF, the RFA is very sensitive to the poles selection, therefore an optimisation is advantageous and improves significantly the curve-fit.

RFA Method	**ERR Q_{hh}**	**Aerodynamic poles Q_{hh}**	**ERR Q_{hg}**	**Aerodynamic poles Q_{hg}**
Standard	1.290E-03	0.057, 0.227, 0.510, 0.907, 1.417	6.716E-01	0.032, 0.128, 0.289, 0.513, 0.802, 1.154
Nelder-Mead	6.422E-04	0.520, 0.689, 0.741, 0.999, 1.001	2.211E-01	0.662, 0.663, 0.668, 0.670, 0.689, 0.693
Genetic Algorithm	5.309E-04	0.633, 0.784, 0.869, 1.041, 1.106	2.228E-01	0.652, 0.658, 0.668, 0.682, 0.683, 0.708
Simulated Annealing	5.135E-04	0.698, 0.899, 0.932, 0.973, 1.189	2.257E-01	0.570, 0.616, 0.626, 0.752, 0.769, 0.770

Table 2: Total approximation error and optimum aerodynamic poles of Q_{hh} and Q_{hg} for different RFA methods

4 PARAMETRIC MODEL ORDER REDUCTION

Model Order Reduction (MOR) techniques have been applied in many engineering fields to replace expensive high fidelity models with low dimensional Reduced Order Models (ROM)

that limit the complexity and computational cost of the simulations, but approximate well the underlying high dimensional systems. For many engineering applications, the governing equations are parameterized and the solution needs to be computed over a potentially large range of parameter values. In the application herein considered, the aeroelastic response of the aircraft must be solved to compute a large number of IQs under different flight conditions, mass configurations and external excitations to show compliance with the certification requirements. The parameters of the aeroelastic equations of motion are thus, for instance, the flight point, altitude and Mach number.

A considerable saving in computational effort is envisaged if, for the thousands of simulations required during an aircraft loads loop, a ROM is used in place of the high dimensional model. The ROM could thus be seen as a physics-based surrogate alternative to data-fit approaches, such as Kriging, Radial Basis Functions, Neural Networks or system identification proposed for the same purpose in [2]. Whereas a data-fit surrogate model, created in a black-box mode, maps an input/output relationship, a ROM embodies the underlying physics of the problem and, unlike the aforementioned methods, its validity is not limited to the conditions under which it was generated, but can be applied to simulate various initial conditions. As the generation of a new ROM at each point of interest in the parameter space is usually impractical, and could even be more computationally expensive than building and evaluating the Full Order Model (FOM) anew, Parametric Model Order Reduction (PMOR) has been introduced to efficiently generate ROMs that preserve the parametric dependency and are accurate over a broad range of parameters, without the need of performing a new reduction at each design point. A survey of the state-of-the-art in PMOR is given in [17].

To present the methodology, the LTI state-space model of the aeroservoelastic system Eq. (2) is written as

$$\begin{aligned} \dot{\boldsymbol{x}} &= \boldsymbol{A}(\boldsymbol{p})\boldsymbol{x} + \boldsymbol{B}(\boldsymbol{p})\boldsymbol{u} \\ \boldsymbol{y} &= \boldsymbol{C}(\boldsymbol{p})\boldsymbol{x} + \boldsymbol{D}(\boldsymbol{p})\boldsymbol{u} \end{aligned} \tag{8}$$

where $\boldsymbol{p} \in \mathbb{R}^d$ is a set of parameters on which the state-space matrices arbitrarily depend and N is the order of the model. MOR seeks a low-dimensional approximation of this dynamic system, of order $n_r \ll N$, through a projection-based reduction

$$\begin{aligned} \dot{\boldsymbol{x}}_{\boldsymbol{r}} &= \boldsymbol{A}_{\boldsymbol{r}}(\boldsymbol{p})\boldsymbol{x}_{\boldsymbol{r}} + \boldsymbol{B}_{\boldsymbol{r}}(\boldsymbol{p})\boldsymbol{u} \\ \boldsymbol{y} &= \boldsymbol{C}_{\boldsymbol{r}}(\boldsymbol{p})\boldsymbol{x}_{\boldsymbol{r}} + \boldsymbol{D}(\boldsymbol{p})\boldsymbol{u} \end{aligned} \tag{9}$$

where

$$\boldsymbol{A}_{\boldsymbol{r}} = (\boldsymbol{W}^T\boldsymbol{V})^{-1}\boldsymbol{W}^T\boldsymbol{A}\boldsymbol{V}, \boldsymbol{B}_{\boldsymbol{r}} = (\boldsymbol{W}^T\boldsymbol{V})^{-1}\boldsymbol{W}^T\boldsymbol{B}, \boldsymbol{C}_{\boldsymbol{r}} = \boldsymbol{C}\boldsymbol{V} \tag{10}$$

The right and left projection matrices $\boldsymbol{W} \in \mathbb{R}^{N\,x\,n_r}$ and $\boldsymbol{V} \in \mathbb{R}^{N\,x\,n_r}$ are referred as the Reduced Order Bases (ROB) and the methods used to calculate these fall into three categories [17]: Krylov subspace methods, balance truncation and proper orthogonal decomposition. In this paper, balanced truncation is chosen to compute the ROB. This is one of the most common techniques employed in the control systems field [18] and it has desirable properties such as stability preservation of the reduced models, an H_∞ error bound and the dimension of the ROM can be easily chosen by observing the decay of the Hankel singular values of the state-space system in balanced form. The right and left bases computed by balanced truncation are the inverse of the other, i.e. $\boldsymbol{W}^T = \boldsymbol{T}_{\boldsymbol{B}}$, $\boldsymbol{V} = \boldsymbol{T}_{\boldsymbol{B}}^{-1}$ and $\boldsymbol{W}^T\boldsymbol{V} = \boldsymbol{I}$.

The idea behind PMOR is the generation of the ROB at a few selected sampling points $\widehat{\boldsymbol{p}}_{\boldsymbol{i}}$ in the parameter domain and then several approaches are possible for constructing a Parametric Reduced Order Model (PROM) at all the other points of interest:

1. Assemble a global basis by collecting the local ROB computed at $\widehat{\boldsymbol{p}}_{\boldsymbol{i}}$ and use this basis to reduce the FOM over the parameter space
2. Interpolate the local ROB to the new unsampled point $\overline{\boldsymbol{p}}$ and perform the reduction
3. Interpolate the locally reduced transfer functions to the new unsampled point $\overline{\boldsymbol{p}}$
4. Interpolate the locally reduce state-space matrices to the new unsampled point $\overline{\boldsymbol{p}}$

The first two approaches are more appropriate if the system has an affine parameter dependency, i.e. the matrices can be explicitly expressed as a function of $\boldsymbol{p}$. The interpolation of the locally reduced transfer functions and of the locally reduced state-space matrices do not suffer from this limitation and thus are more convenient for a generic non-affine parameter dependency, which is indeed the case of the aeroservoelastic system of Eq. (1). In this work, the approach of PMOR by state-space matrices interpolation is chosen. This method has been successfully applied in the past in aeroelasticity, for fast flutter clearance of a wing-store configuration [19], in control system design of a flexible aircraft [20], in unsteady CFD [21], but not for gust and manoeuvre loads prediction. Hereafter, the PMOR framework proposed in [22] is followed. It consists of the following steps:

1. Generation of the n_p local ROMs at the sampling points $\widehat{\boldsymbol{p}}_{\boldsymbol{i}}$, $i = 1 \dots n_p$
2. Congruence transformation of the locally reduced state-space matrices
3. Elementwise interpolation of the locally reduced state-space matrices to the validation points $\overline{\boldsymbol{p}}$
4. Time simulation of the resulting interpolated ROM

In the first step, the parameter space is sampled, the FOMs constructed at each of these points and then individually reduced through balanced truncation. All the local ROMs have the same order n_r. For the aeroservoelastic system under consideration this task is quite challenging because the state matrix is poorly conditioned, lightly damped and neutrally stable poles are present (rigid body modes). Moreover, to achieve a significant computational time saving, the sampling grid must be coarse, whereas the altitude and airspeed affect considerably the dynamics of the aircraft.

As balanced truncation is not a physics-based reduction, such as the modal condensation, but a purely mathematical one, the states of the ROMs at different parameter values lie in unrelated subspaces and, before the interpolation, must be transformed, through a similarity transformation $\boldsymbol{x}_{\boldsymbol{r},i} = \boldsymbol{P}_i \widehat{\boldsymbol{x}_{\boldsymbol{r},i}}$, to a congruent common subspace, spanned by the column of the matrix $\boldsymbol{R} \in \mathbb{R}^{N\, x\, n_r}$. The choice of this reference subspace is critical for the accuracy of the entire procedure, it is problem-dependent and various options have been proposed [19]. A solution that, for the application considered, is robust and delivers accurate results is adopting as the reference subspace $\boldsymbol{R}$ the first n_r singular vectors of the matrix $\boldsymbol{V_{all}}$ which collects all the local ROB $\boldsymbol{V}_i = \boldsymbol{T}_{\boldsymbol{B},i}^{-1}$ [17], that is

$$\begin{gathered} \boldsymbol{V_{all}} = \left[\boldsymbol{V_1}\ \boldsymbol{V_2} \dots \boldsymbol{V_{n_p}}\right] = \boldsymbol{U\Sigma Z}^T \\ \boldsymbol{R} = \boldsymbol{U}_{1:n_r} \end{gathered} \tag{11}$$

where first the matrices $\boldsymbol{T}_{\boldsymbol{B},\boldsymbol{i}}^{-1}$ are orthonormalized to limit the loss of accuracy due to this further transformation. The transformation matrix $\boldsymbol{P}_i$, for each local ROM, is computed by the minimization problem [17]

$$\min_{\boldsymbol{P}_i} \|\boldsymbol{V}_i\boldsymbol{P}_i - \boldsymbol{R}\|_F^2 \qquad s.t. \;\; \boldsymbol{P}_i{}^T\,\boldsymbol{P}_i = \boldsymbol{I} \tag{12}$$

whose solution is obtained through SVD as

$$\begin{aligned} \boldsymbol{U}_{\boldsymbol{V}_i}\boldsymbol{\Sigma}_{\boldsymbol{V}_i}\boldsymbol{Z}_{\boldsymbol{V}_i}^T &= svd(\boldsymbol{V}_i\boldsymbol{R}) \\ \boldsymbol{P}_i &= \boldsymbol{U}_{\boldsymbol{V}_i}\boldsymbol{Z}_{\boldsymbol{V}_i}^T \end{aligned} \tag{13}$$

The congruence transformed local ROM are given by

$$\widehat{\boldsymbol{A}_{\boldsymbol{r},\boldsymbol{i}}} = \boldsymbol{P}_i{}^T\boldsymbol{T}_{\boldsymbol{B}}\boldsymbol{A}(\widehat{\boldsymbol{p}_{\boldsymbol{i}}})\boldsymbol{T}_{\boldsymbol{B},\boldsymbol{i}}^{-1}\boldsymbol{P}_i,\;\; \widehat{\boldsymbol{B}_{\boldsymbol{r},\boldsymbol{i}}} = \boldsymbol{P}_i{}^T\boldsymbol{T}_{\boldsymbol{B}}\boldsymbol{B}(\widehat{\boldsymbol{p}_{\boldsymbol{i}}}),\;\; \widehat{\boldsymbol{C}_{\boldsymbol{r},\boldsymbol{i}}} = \boldsymbol{C}(\widehat{\boldsymbol{p}_{\boldsymbol{i}}})\boldsymbol{T}_{\boldsymbol{B},\boldsymbol{i}}^{-1}\boldsymbol{P}_i \tag{14}$$

Once all the local reduced models are available in this form, the resulting PROM at $\overline{\boldsymbol{p}}$ is obtained by direct interpolation of the matrices in Eq. (14). The interpolation is performed element-by-element through a linear or cubic spline interpolant. This step is the other main source of possible inaccuracy of the procedure, besides the reduction itself.

5 APPLICATION TO GUST AND MANOEUVRE LOADS PREDICTION

Certification requirements specify the discrete gust load cases considering the aircraft in level flight subject to symmetrical vertical and lateral gusts with a "1-cosine" velocity profile having gust gradient H (half of the gust wavelength) and asking for several gust gradients between 30ft and 350ft to be investigated in order to determine the critical conditions [1]. Regarding pitching manoeuvres, the certification specifications cover unchecked and checked abrupt pitching manoeuvres [1]. The abrupt unchecked pitching involves, with the aircraft in steady flight up to V_A, a sudden displacement of the elevator so as to yield the maximum positive load factor; the response needs not to be considered after this limit, or the maximum tail load, has been reached. The checked pitching manoeuvre, starting with the aircraft in steady flight between V_A and V_D, considers both nose-up and nose-down pitching obtained applying a sinusoidal displacement of the elevator tuned to achieve, and not exceed, the positive limit load factor, for initial nose-up manoeuvres, or a load factor of 0g, for initial nose-down manoeuvres.

The PROM methodology presented is applied to simulate all the gust and pitching manoeuvre load cases across the flight envelope (altitude vs. Mach). To assemble the state-space model Eq. (2) for the flight envelope sweep, the first 30 normal modes are retained and the RFAs of $\boldsymbol{Q}_{\boldsymbol{hh}}$ and $\boldsymbol{Q}_{\boldsymbol{hg}}$ performed with respectively 5 and 6 aerodynamic poles optimised using a Genetic Algorithm. The full aeroservoelastic state-space model features 390 states and three inputs, namely gust velocity and its time derivative and pilot elevator command.

5.1 Results

The 16 flight conditions (sampling points) used to generate the ROMs for the interpolation are shown in Figure 2, along with the 156 conditions used to sweep the whole flight envelope (validation points). Through balanced truncation, the number of states is reduced from 390 to 34. The reduced state-space matrices are interpolated elementwise through a simple yet efficient bilinear interpolant and FOMs are constructed at each validation point to assess the

accuracy of the procedure. Gust response, considering ten gust gradients, and pitching manoeuvres simulation are then performed using a state-transition matrix integration method.

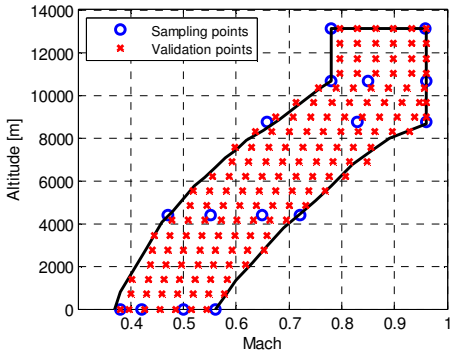

Figure 2: Sampling points and validation points in the flight envelope

Figure 3 shows a comparison between the exact time histories, at five different flight conditions and for a fixed gust gradient, of the wing root bending moment and of the wing inboard engine section torque obtained with the FOM and with the PROM. The agreement of both the peak values and of the decay is very good. To assess the accuracy of the procedure, the errors, with respect to the FOM, of the maximum and minimum wing root bending moment and wing inboard engine section vs. Mach number and altitude are presented in Figure 4. The predictions are very good, the error in the whole flight envelope being less than ±3%. The accuracy is slightly worse for the torque because the torsional modes have higher frequencies than the bending modes and hence are more sensitive to the states truncation. This error is anyhow introduced by the balanced truncation itself rather than by the interpolation.

The approximation errors are in line with those presented in [3], where Neural Networks and system identification were used as black-box surrogates to approximate the extreme responses. However, following this approach, a different metamodel must be built for each IQ, a cost that could quickly become unacceptable for an industrial case where thousands of IQs are monitored. The present methodology, on the other hand, is more flexible since this need is achieved by just adding a row in the $\boldsymbol{C}$ and $\boldsymbol{D}$ matrices of the output equations. In addition, the number of sampling points required to generate an accurate PROM is considerably lower than that needed by data-fit surrogates [2].

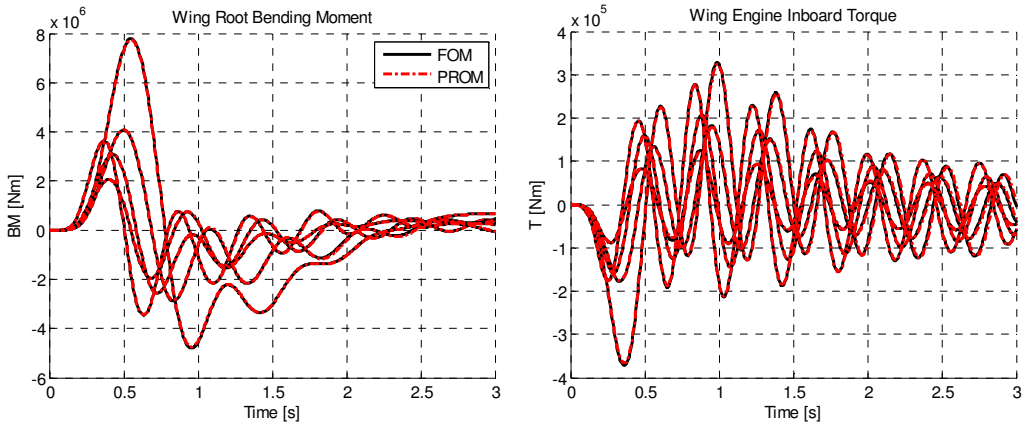

Figure 3: Wing root bending moment and wing inboard engine torque time responses at different flight conditions, FOM vs. PROM

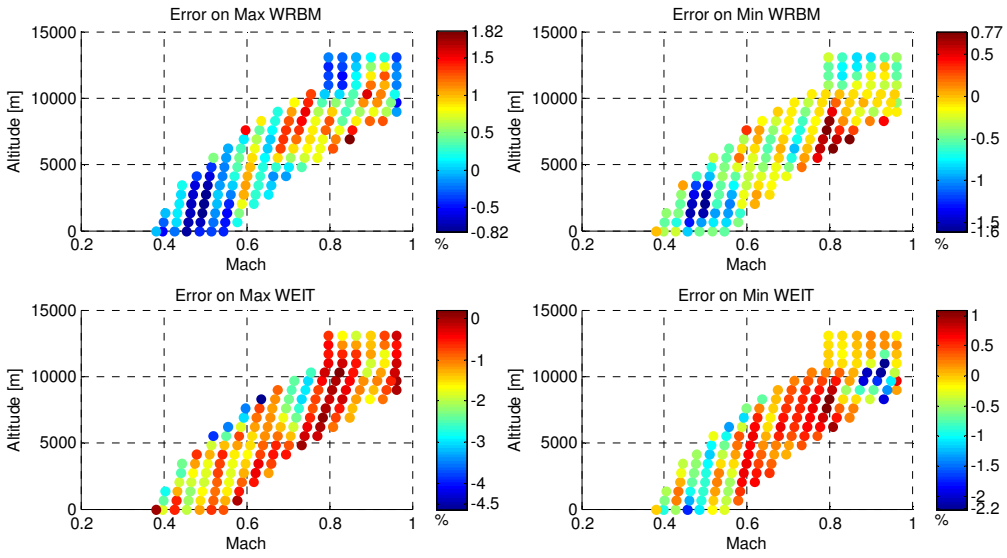

Figure 4: Percentage error on the Max/Min prediction of the wing root bending moment and wing inboard engine torque

A more challenging goal is the efficient approximation of correlated loads plots. Figure 5 shows the correlated loads plots, bending moment vs. torque, of a gust family at the root and inboard engine wing sections obtained with the FOM and the PROM at two flight conditions. The prediction obtained with the PROM, as for 1D IQs, is in excellent agreement with the FOM computations.

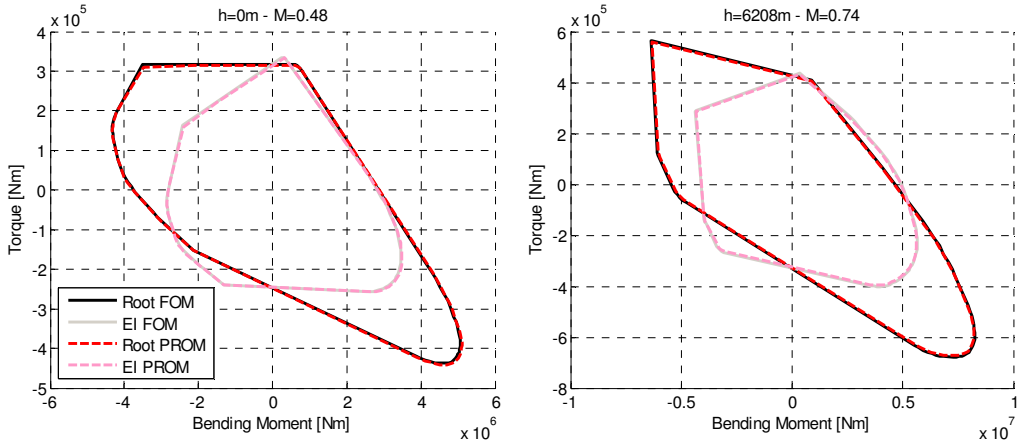

Figure 5: Correlated loads plots (bending vs. torque) at the wing root and inboard engine wing section at two flight conditions, FOM vs. PROM

Similarly, simulations of unchecked and checked abrupt pitching manoeuvres are performed with the PROM and FOM. The time histories of the incremental load factor during a nose-up and nose-down checked pitching manoeuvre are shown in Figure 6, at sea level and Mach 0.40, alongside with the bending moment and torque at the horizontal tail root. A very good match is obtained for these load cases too, as confirmed by the correlated loads plots of the wing root and horizontal tail root presented in Figure 7.

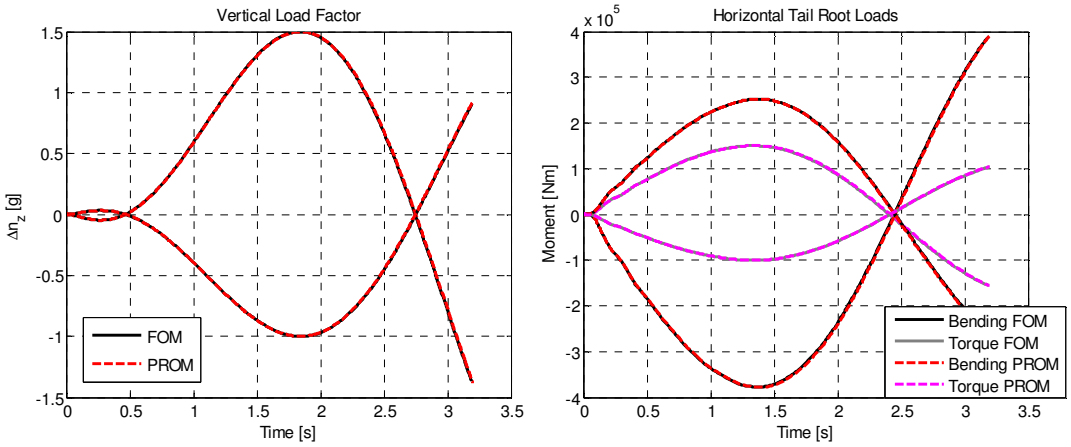

Figure 6: Load factor and horizontal tail root loads for nose-up and nose-down checked pitching manoeuvre at h=0m – M=0.40, FOM vs. PROM

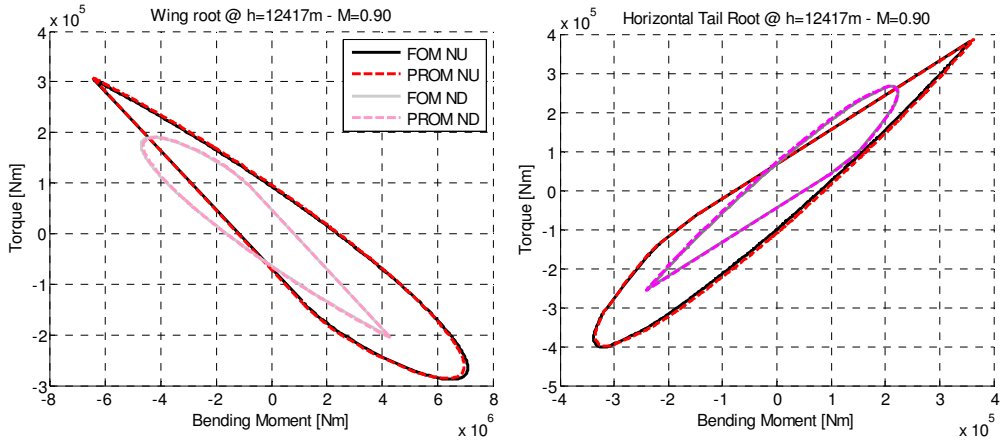

Figure 7: Correlated loads plots (bending vs. torque) at the wing root and horizontal tail root for nose-up and nose-down checked pitching manoeuvre at h=12417m – M=0.90, FOM vs. PROM

For all the load conditions considered, the agreement between the FOM and PROM is excellent, demonstrating that the proposed method can deliver accurate predictions for a considerable saving in computational effort. The saving increases with the number of simulations to be performed, as shown in Figure 8: for the complete sweep of the flight envelope, considering ten gust gradients, the PROM requires just 11% of the FOM computational time.

A breakdown of the computational time is presented in Figure 8. Whereas for the FOM most of the computational time is spent doing the actual simulation, for the PROM this makes up only 34% of the total time, the greatest part being spent in the calculation of the balanced truncation of the state-space models at the sampling points. The congruence transformation and matrix interpolation instead account for a negligible fraction of the total. Since each balanced truncation involves the solution of two Lyapunov equations, whose computation cost is $o(N^3)$, and the time integration the creation of the $\boldsymbol{A}$ matrix exponential and repeated matrix-vector products, $o(sn_r{}^3) + o(2n_t n_r{}^2)$, the need to minimise and optimise the number and location of the sampling points is clear.

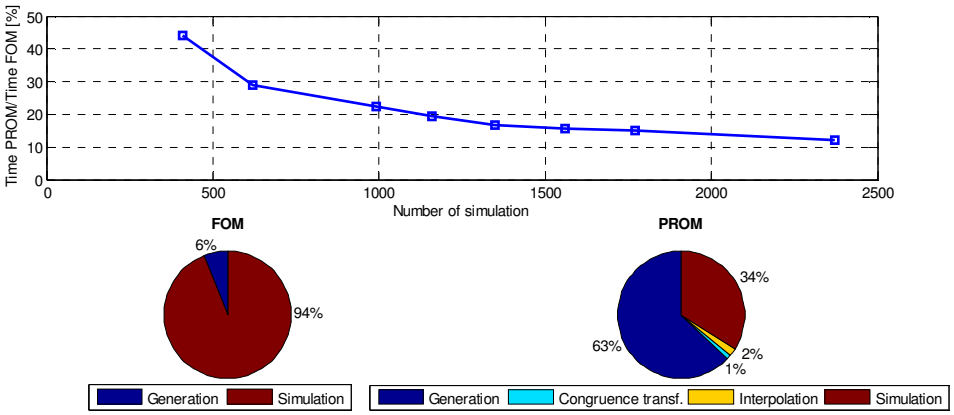

Figure 8: Ratio of PROM and FOM total computational time required and breakdown

6 SIMULATION OF CONCENTRATED STRUCTURAL NONLINEARITIES

Typically two approaches have primarily been applied in the past to predict the transient response of aeroelastic systems with structural nonlinearities: harmonic balance method and direct numerical simulation in time-domain [6]. The latter can deal with generic types of nonlinearities, not only concentrated ones as the former, and is able to capture the whole dynamic behaviour of the system, whereas the harmonic balance method has limitations in this regard [23].

In this work, the PMOR framework is extended to deal with concentrated structural nonlinearities. Since it requires the equations to be in time-domain, the direct simulation approach is applied and the nonlinear aeroelastic system approximated as a series of piecewise linear ones, where the nonlinearity is treated as a parameter of the system. The main idea behind is to consider the parameter p of the PROM Eq. (9) as a nonlinear property of the model which can be calculated from the states of the system and monitored during the time response. The matrices of the aeroelastic state-space ROM are not constant anymore throughout the response, but dependent on the actual configuration of the system via the nonlinear property p. At each time step t_i of the integration, an updated ROM is built by interpolation according to the current value of $p(t_i)$ and used for the next time step. Thus a nonlinear system is simulated by switching between sub-linear ones. Compared to a fully nonlinear analysis, this piecewise-linear approach is on the one hand an approximation, and on the other a more computationally efficient way and relies on the standard linear aeroelastic tools commonly employed in the industrial practice, without the need of resorting to nonlinear aeroelastic solvers which, on the contrary, are not readily available.

Similar methods have been proposed in the electrical engineering field, where it is known as Trajectory Piecewise-Linear (TPWL) [25], and in multibody dynamics [26], where it is known as Global Modal Parameterization (GMP). In the aeroelasticity field, Chen et al. [27] present a time simulation method based on the interpolation and switching of discrete linear state-space models and apply it to study the aeroelastic stability of an airfoil with freeplay and of a joined wing aircraft subject to buckling. The state-space models are however FOMs, not ROMs as herein proposed. Considering the size of a FOM and the need for the interpolation and switching at each time step, the usage of a ROM is envisaged to be more efficient, especially when used in an optimisation loop.

In the following section, the introduction of concentrated structural nonlinearities starting from a linear aeroelastic model, based on a FE discretization, is presented. The choice of a suitable generalized basis to formulate the equations is discussed and then the solution procedure described.

6.1 Modelling of concentrated structural nonlinearities

In industrial practice, aeroelastic analyses are still routinely performed using linear models and tools. Nonlinear aeroelastic solvers are not readily available and the alternative approach is a co-simulation between a nonlinear structural solver and an aerodynamic solver, which leads to a considerable increase in complexity and computational time. The method proposed in this work to simulate concentrated structural nonlinearities considers a linear piecewise discretization of the arbitrary non linearity based on the current configuration of the system throughout the transient response. In this way, a nonlinear system is simulated as a series of piecewise LTI systems that can be generated with standard aeroelastic tools.

Considering, without loss of generality, a cubic nonlinear force-displacement relation of a flexible element of the FE model of the structure, a linearized equivalent stiffness can be computed as

$$K\big(\theta(t)\big) = K_0 + K_{nl}\theta^2(t) \tag{15}$$

where K_0 is the linear part of the stiffness and θ the Degree Of Freedom (DOF) where the non linearity acts. During the nonlinear response, changes in stiffness occur based on the actual value of θ. In a linearized fashion, these can be represented as an incremental stiffness matrix $\Delta\boldsymbol{K}$ to be added to the stiffness matrix of the linear model $\boldsymbol{K_0}$ at each time step of the integration based on the current deflection $\bar{\theta}$. As the nonlinearity is concentrated, $\Delta\boldsymbol{K}$ is a low rank matrix with zeros everywhere except for the DOFs where the nonlinear element is located. The actual stiffness, projected in the generalized subspace by $\boldsymbol{\Phi}$, is then given by

$$\boldsymbol{K_{hh}}(\bar{\boldsymbol{\theta}}) = \boldsymbol{\Phi^T}[\boldsymbol{K_0} + \Delta\boldsymbol{K}(\bar{\boldsymbol{\theta}})]\boldsymbol{\Phi} \tag{16}$$

Thus, following this approach, the nonlinear aeroelastic state-space system is approximated by a set of linearized LTI systems parameterized by the nonlinear physical DOF θ as

$$\begin{aligned} \dot{\boldsymbol{x}}_{\boldsymbol{ae}}(\boldsymbol{\theta}) &= \boldsymbol{A_{ae}}(\boldsymbol{\theta})\boldsymbol{x_{ae}}(\boldsymbol{\theta}) + \boldsymbol{B_{ae}}(\boldsymbol{\theta})\boldsymbol{u} \\ \boldsymbol{y}(\boldsymbol{\theta}) &= \boldsymbol{C_{ae}}(\boldsymbol{\theta})\boldsymbol{x_{ae}}(\boldsymbol{\theta}) + \boldsymbol{D_{ae}}(\boldsymbol{\theta})\boldsymbol{u} \end{aligned} \tag{17}$$

6.2 Generalized basis with structural nonlinearities

An issue for aeroelastic systems with structural nonlinearities is the choice of an adequate generalized basis to formulate the equations of motion. As the structure is nonlinear, a unique set of normal modes does not strictly exist anymore, but it changes according to the configuration of the structure. For this reason, it is necessary to select a unique generalized basis capable of representing the physical displacements in the entire domain of the nonlinear response. A number of methods have been proposed for this purpose: in/out bases [23], the fictitious mass method [28], the residual vectors method [24]. These latter two approaches are suitable when dealing with a generic concentrated nonlinearities, not limited to freeplay, and the concept, though practically obtained in different ways, is the same, that is augmenting the

normal modes with shape vectors containing significant local deformation at the DOFs where the concentrated nonlinearities act.

In this work, the residual vectors method is applied. It consists of adding to the normal modes of a baseline configuration (for the nonlinear case assumed to be the aircraft in the undeformed condition) shape vectors corresponding to a unit displacement (or rotation) of the DOF where the nonlinearity is located, computed by a static solution. A reorthogonalization of the augmented basis to the baseline mass and stiffness matrices is then performed to remove redundant components and obtain a basis which diagonalizes the baseline mass and stiffness matrices. The addition of the residual vectors to the basis comprising the normal modes produces high frequency synthetic modes representing the local deformation in the proximity of the DOFs of interest. The static participation of these high frequency shapes is paramount in achieving accuracy whereas the dynamic response could generate spurious oscillations that do not represent the physical response of the structure. To overcome this pitfall, critical damping is assigned to these synthetic modes.

6.3 Solution procedure

The solution procedure consists of the following steps:

1. A database of congruence transformed linear ROMs is generated in an off-line phase for a discrete set of values of the linearized equivalent stiffness $\widehat{K}_j$ and a fixed flight condition
2. The time integration starts from the initial conditions using a state-transition matrix integration method
3. The value of the linearized equivalent stiffness at the current time step t_i is calculated based on the actual deflection $\theta(t_i)$, recovered from the states $\boldsymbol{x_r}(t_i)$
4. The updated ROM matrices $\boldsymbol{A_r}(\theta(t_i))$, $\boldsymbol{B_r}(\theta(t_i))$, $\boldsymbol{C_r}(\theta(t_i))$, $\boldsymbol{D_r}(\theta(t_i))$ are calculated by interpolation from the database generated off-line at step 1
5. The updated ROM is used for the next integration step t_{i+1}.

The selection of the sampling points for the linearized equivalent stiffness is critical for the accuracy of the procedure. These must cover the entire expected range of variations during the nonlinear response and must be fine enough to limit the interpolation error. Since the matrices interpolation and switching is performed at each time step, the number of interpolations can be significantly high, depending of course on the length of the time history and on the size of the time step for the integration. Thus, the benefit of using a ROM instead of a FOM is clear, especially when several flight conditions must be analysed for loads prediction, or if the nonlinear transient response is used in an optimisation run.

6.4 Optimisation of a nonlinear wing tip device

The PROM framework for aeroelastic systems with structural nonlinearities is applied to the optimisation of a passive nonlinear wing tip device for load alleviation which was first presented by one of the authors in [30]. The wing tip device concept is shown in Figure 9. Its main purpose is to extend the wingspan in order to achieve a reduction in induced drag and, eventually, in fuel consumption. This goal conflicts with the increase in loads and, as a result, in structural weight caused by a span extension. A system is then devised to embed in the

wing tip a passive load alleviation function by connecting it to the outboard wing through a flexible element, located ahead of the wing tip's centre of pressure, whose torsional stiffness is tuned to provide alignment of the wing tip and the main wing in cruise flight and to allow the pitching motion of the device, in the direction of a load reduction, at increasing load levels.

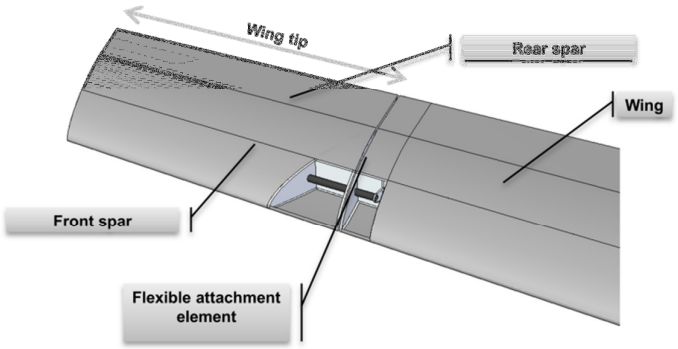

Figure 9: Wing tip device for passive load alleviation [30]

The original design of the wing tip [30] features a flexible attachment element with a linear stiffness, which was selected to maximise the wing bending moment alleviation, with respect to a rigid wing span extension, via a constrained gradient-based optimisation with flutter constraints, as the device can induce wing flutter. In this paper, the stiffness of the attachment element is considered nonlinear and nonlinear gust responses simulated with the PROM approach previously introduced. A cubic restoring force of the attachment element in the torsional DOF θ is assumed, which leads to the linearized equivalent stiffness of Eq. (15)

$$K\big(\theta(t)\big) = K_0 + K_{nl}\theta^2(t) \tag{15}$$

where the two coefficients K_0 and K_{nl} define respectively the linear and the nonlinear (cubic) contribution to the restoring force.

As shown in [30] for the linear design, the more flexible the attachment element, the greater the bending moment alleviation achieved. However, this effect results in an excessive misalignment of the wing tip in cruise, which could increase the interference drag and drag due to flow separation, offsetting the reduction in induced drag obtained with the span extension. A multi-objective optimisation of the nonlinear stiffness is therefore carried out, assuming as design variables K_0 and K_{nl}, and two conflicting objective functions, properly normalised, are identified:

1. Minimisation of worst case Max/Min wing bending moment along the wingspan with respect to the linear design

$$\mathcal{F}_1 = {}^1\!/_{I_S} \sum_{j=1}^{n_{sec}} \left(\frac{BM_{max,j}^{NL}}{BM_{max,j}^{LIN}} + \frac{BM_{min,j}^{NL}}{BM_{min,j}^{LIN}} \right) \tag{18}$$

2. Minimisation of the wing tip misalignment $\theta_{1g,k}$ in cruise conditions

$$\mathcal{F}_2 = {}^1\!/_{M} \sum_{k=1}^{M} \left(\frac{|\theta_{1g,k}|}{\bar{\theta}_{1g}} \right) \tag{19}$$

For the optimisation a set of M flight conditions covering the whole flight envelope is considered. Trim analyses in cruise at 1g, with static aeroelastic effects, and gust responses are performed at all the selected flight conditions, since gust loads are typically the critical load cases for the wing of a modern airliner. Because the system under consideration is nonlinear, the gust response depends on the initial 1g trim condition and loads due to the gust and to cruise flight cannot be calculated independently and superimposed as done in linear analysis. Thus, in the optimisation process, for each flight condition a nonlinear trim analysis is first performed to calculate the initial wing tip relative deflection and wing loads and then this solution is used as the initial condition for the time integration of the nonlinear gust response.

The entire procedure for predicting the transient response, including a concentrated structural non linearity and optimisation using the PROM, is shown in Figure 10. The advantage of using the PROM methodology is twofold: a complete sweep of the flight envelope and the identification of the worst case gust for each wing section can be rapidly performed without the need of generating and using for the simulation a new FOM at each flight condition By simply interpolating the database of ROMs generated in an off-line phase, and the same reduction and interpolation procedure is used to sample the linearized equivalent stiffness, generating a database of sub-linear ROMs to carry out the nonlinear trim and gust response in a piecewise-linear manner.

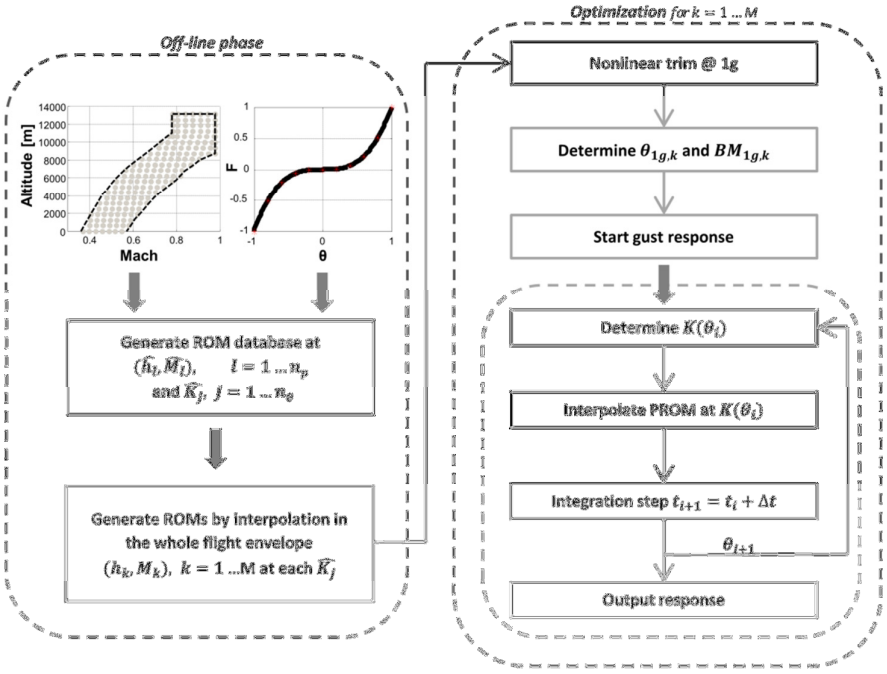

Figure 10: Flowchart of the nonlinear wing tip simulation and optimisation procedure

6.4.1 Results

The wing tip device considered increases the wing span by 10% and the attachment element is located at 24% of the root chord with its axis perpendicular to the airstream. The optimisation is performed using a Multi-Objective Genetic Algorithm. As the system is nonlinear, a classical p-k flutter analysis cannot be performed, therefore freedom from flutter is ensured by

checking if any of the modal coordinates, monitored in the output vector $\boldsymbol{y}$, tend to diverge during the gust response.

The Pareto front of the multi-objective optimisation is shown in Figure 11. The Pareto-optimal solutions show a greater variability in the misalignment objective function whereas the load alleviation is less sensitive to the stiffness coefficients. The solution chosen on the Pareto front is highlighted (coefficients normalized to the linear torsional stiffness equal to 33000Nm/rad from [30]). The linear stiffness coefficient is increased almost to its upper bound (set to 1.2), basically to limit the cruise misalignment. This is expected as in cruise, due to the lower lift acting on the wing, the wing tip operates around θ=0deg where the stiffness curve is dominated by the linear term. As the aerodynamic load increases due to a gust encounter, the wing tip deflects and operates in the nonlinear region. Since a more flexible device is more effective in alleviating the loads, the optimal solution features a negative nonlinear stiffness coefficient, i.e. a softening effect. From a practical point of view, a softening effect can occur in a structural element undergoing buckling [6].

As an example, the time history of the incremental bending moment due to the worst case positive gust at two wing sections is shown in Figure 12, for the aircraft equipped with the nonlinear and the linear wing tip. The additional flexibility introduced by a nonlinear stiffness achieves a reduction of the maximum and minimum peak loads. This is caused by the increased nose-down deflection of the wing tip with nonlinear stiffness under loads with respect to the linear design (+31% deflection), as shown in Figure 13, which also presents how the linearized stiffness decreases throughout the response thanks to the softening effect.

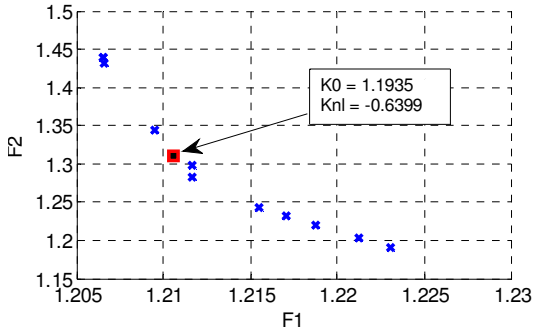

Figure 11: Pareto front of the genetic optimisation procedure and selected individual

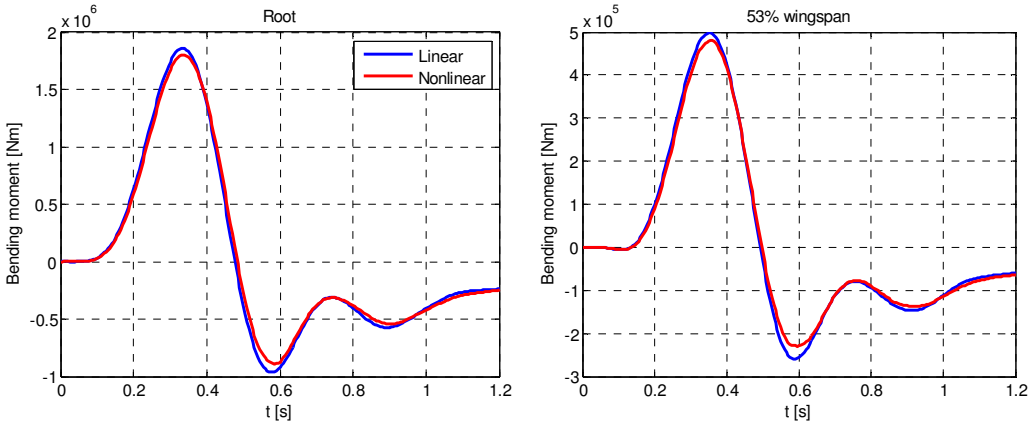

Figure 12: Bending moment for worst case positive gust at the root and at 53% wingspan, linear vs. nonlinear

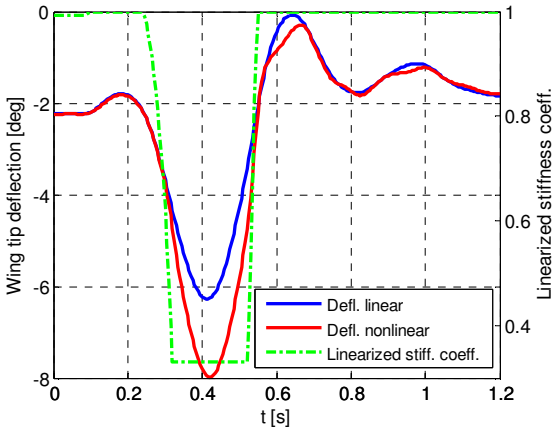

Figure 13: Wing tip deflection linear vs. nonlinear and equivalent linearized stiffness for worst case positive gust

To assess the behaviour of the device in the entire flight envelope, the ratio of the maximum bending moment of the nonlinear and linear design is computed and presented in Figure 14 for two wing sections. For all the flight conditions, the optimised nonlinear device is capable of further reducing the loads compared to the linear one; the alleviation, though limited at the root, increases towards the outboard wing, an important consideration because this is the area that typically requires structural reinforcements due to a span extension [30].

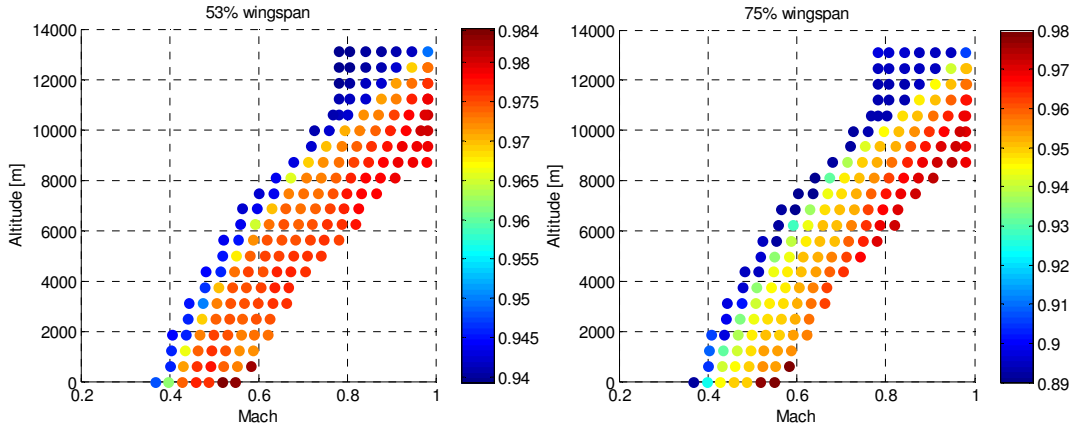

Figure 14: Maximum bending moment alleviation (ratio nonlinear/linear) in the flight envelope at two sections

7 CONCLUSIONS

In this paper, a method based on a Parametric Reduced Order Model has been applied to rapidly predict gust and manoeuvre loads of an aircraft aeroservoelastic model. It has been shown that both Max/Min and correlated loads are accurately predicted achieving a significant saving in computational time. The same methodology has been extended to simulate the transient response of aeroelastic systems with concentrated structural nonlinearities. The procedure relies on the standard linear aeroelastic tools still commonly employed in the industry and performs the simulation in the time-domain of the nonlinear aeroelastic system in a piecewise-linear fashion, switching between sub-linear reduced order systems, obtained by interpolation, according to the current configuration of the states. The

methodology has been applied to study the behaviour of a passive wing tip device for load alleviation with a nonlinear stiffness and comparing it to a linear one. A multi-objective optimisation has been carried out to tune the nonlinear stiffness subject to load alleviation and aerodynamic objectives in the whole flight envelope, showing the effectiveness and efficiency of the proposed methodology.

8 REFERENCES

[1] EASA, Certification Specification for Large Aeroplanes CS-25 Amendment 3, September 2007.

[2] Khodaparast, H. H., Georgiu, G., Cooper, J. E., Riccobene, L., Ricci, S., Vio, G. A., and Denner, P., Efficient worst case 1-cosine gust loads prediction, *ASD Journal*, 2012, 2(3), pp. 33-54.

[3] Cavagna, L., Ricci, S., Riccobene, L., FAST-GLD: a fast tool for the prediction of worst case gust loads based on neural networks, *Proceedings of 54th AIAA/ASME/ASCE/AHS/ASC Structures, Structural Dynamics and Materials Conference*, Boston, MA, 2013.

[4] Khodaparast, H. H., Cooper, J. E., Worst case gust loads prediction using surrogate models and system identification methods, *Proceedings of 54th AIAA/ASME/ASCE/AHS/ASC Structures, Structural Dynamics and Materials Conference*, Boston, MA, 2013.

[5] Tartaruga, I., Sartor, P., Cooper, J. E., Coggon, S., Lemmens, Y., Efficient prediction and uncertainty propagation of correlated loads, *Proceedings of 56th AIAA/ASME/ASCE/AHS/ASC Structures, Structural Dynamics and Materials Conference*, Orlando, FL, 2015.

[6] Lee, B. H. K., Price, S. J., Wong, Y. S., Nonlinear aeroelastic analysis of airfoils: bifurcation and chaos, *Progress in Aerospace Sciences*, 1999, 35(3), pp. 205-334.

[7] Albano, E., Rodden, W. P., A doublet-lattice method for calculating lift distributions on oscillating surfaces in subsonic flows, *AIAA Journal*, 1969, 7(2), pp. 279-285.

[8] Merrit, H. E., Hydraulic control systems, Wiley, 1967.

[9] Tiffany S. H., Karpel M., Aeroservoelastic modelling and applications using the minimum-state approximations of the unsteady aerodynamics, NASA TM-101574, 1989.

[10] Roger, K. L., Airplane math modeling methods for active control design, AGARD CP-228, 1977.

[11] Karpel, M., Design for active and passive flutter suppression and gust alleviation, NASA CR-3482, 1981.

[12] Ripepi, M., Mantegazza, P., Improved matrix fraction approximation of aerodynamic transfer matrices, *AIAA Journal*, 2013, 51(5), pp. 1156-1173.

[13] Karpel, M., Moulin, B., Chen, P. C., Dynamic Response of Aeroservoelastic Systems to Gust Excitation, *Journal of Aircraft*, 2005, 42(5), pp. 1264-1272.

[14] Tiffany, S. H., Adams, W. M., Jr., Nonlinear programming extensions to rational function approximation for unsteady aerodynamic forces, NASA TP-2776, 1988.

[15] Karpel, M., Strul, E., Minimum-state unsteady aerodynamic approximations with flexible constraints, *Journal of Aircraft*, 1996, 33(6), pp. 1190-1196.

[16] Berci, M., Optimal approximation of indicial aerodynamics, *Proceedings of the1st International Conference on Engineering and Applied Sciences Optimisation*, National Technical University of Athens, Athens, 2014, pp. 1241-1277.

[17] Benner, P., Gugercin, S., Willcox, K., A survey of model reduction methods for parametric systems, *Max Planck Institute Magdeburg Preprints*, 2013.

[18] Moore, B., Principal component analysis in linear systems: Controllability, observability and model reduction, *IEEE Transactions on Automatic Control*, 1981, 26, pp. 17-32.

[19] Amsallem, D., Farhat, C., Interpolation method for the adaption of reduced-order models to parameter changes and its application to aeroelasticty, *AIAA Journal*, 2008, 46(7), pp. 1803-1813.

[20] Poussot-Vassal, C., Roos, C., Generation of a reduced-order LPV/LFT model from a set of large-scale MIMO LTI flexible aircraft models, *Control Engineering Practice*, 2012, 20(9), pp. 919-930.

[21] Zimmermann, R., A locally parametrized reduced-order model for the linear frequency domain approach to time-accurate computational fluid dynamics, *SIAM Journal on Scientific Computing*, 2014, 36(3), pp. 508-537.

[22] Panzer, H., Mohring, J., Eid, R., Lohmann, B., Parametric model order reduction by matrix interpolation, *at-Automatisierungstechnik*, 2010, 58(8), pp. 475-484.

[23] Arevalo F., Garcia-Fogeda P., Climent H., Nonlinear time-domain structure/aerodynamics coupling in systems with concentrated structural nonlinearities, *Proceedings of the 27th International Congress of the Aeronautical Sciences*, 2010.

[24] Silva G. H. C., Dal Ben Rossetto G., Dimitriadis G., Reduced order analysis of aeroelastic systems with freeplay using an augmented modal basis, *Journal of Aircraft* (in press)

[25] Rewienski, M., White, J., A trajectory piecewise-linear approach to model order reduction and fast simulation of nonlinear circuits and micromachined devices, *IEEE Transactions on Computer-Aided Design of Integrated Circuits and Systems*, 2003, 22(2), pp. 155-170.

[26] Brüls, O., Duysinx, P., Golinval, J. C., The global modal parameterization for non-linear model-order reduction in flexible multibody dynamics, *International Journal for Numerical Methods in Engineering*, 2007, 69(5), pp. 948-977.

[27] Chen, P. C., Sulaeman, E., Nonlinear response of aeroservoelastic systems using discrete state-space approach, *AIAA Journal*, 2003, 41(9), pp. 1658-1666.

[28] Karpel, M., Strul, E., Time simulation of flutter with large stiffness changes, *Journal of Aircraft*, 1994, 31(2), pp. 404-410.

[29] Rose, T., Using Residual Vectors in MSC/NASTRAN Dynamic Analysis to Improve Accuracy, *Proceedings of MSC World Users' Conference*, 1991.

[30] Ricci, S., Castellani, M., Romanelli, G., Multi-Fidelity Design of Aeroelastic Wing Tip Devices, *Proceedings of the Institution of Mechanical Engineers Part G: Journal of Aerospace Engineering*, 2012, 227(10), pp. 1596-1607.

9 COPYRIGHT STATEMENT